

HIGH-RESOLUTION TARGET SENSING USING MULTI-FREQUENCY SPARSE ARRAY

Ammar Ahmed, Dennis Silage, Yimin D. Zhang

Department of Electrical and Computer Engineering, Temple University, Philadelphia, PA 19122, USA

ABSTRACT

In this paper, we discuss high-resolution target sensing through the exploitation of multi-frequency sparse array processing. By using simple design examples of a three-element sensor array coupled with the sensing signals consisting of three well-designed frequencies, we provide insights to achieve a high number of consecutive lags, unique lags, and array aperture. Such multi-frequency sensor arrays with reduced number of sensors can be attractive in many applications to achieve effective sensing with a low cost.

Index Terms— Sparse array, multi-frequency sensing, group sparsity, DOA estimation.

1. INTRODUCTION

Sparse array design and the associated signal processing methods have attracted significant research interests because of their desirable capabilities to achieve $O(N^2)$ degrees-of-freedom (DOFs) using only N sensors [1, 2]. Recently, inspired by the coprime and nested array structures [3–5], a number of systematical sparse array design schemes have been developed [6–16]. A class of direction-of-arrival (DOA) estimation methods applied on sparse arrays have been developed based on the MUSIC as well as compressive sensing methods [6, 9, 15, 17–19].

In [20], the concept of constructing a virtual coprime array using a uniform linear array (ULA) with two frequencies that are associated with a coprime relationship was developed. This extends the coprime array and filter concept in either the spectral or spatial domain to a joint spatio-spectral domain, thereby achieving high flexibility in array structure design to meet both DOF and system complexity constraints. The extension to multiple coprime frequencies, together with the analysis of the achievable number of DOFs, are provided in [21–25]. In [26], the Cramer-Rao lower bound of the dual-frequency coprime array is analyzed. It is pointed out in [26] that such arrays can resolve signals that have identical DOAs or with close spatial separations.

In this paper, we consider a general framework of multi-frequency sparse arrays at the node level which can be further applied to distributed sensing. In such a system, the multi-frequency sensing signals may be emitted by a distant transmitter with adequate power resources, whereas the receiver

array is located at the passive sensor nodes which are low-cost and stealthy.

Compared to the previous coprime-frequency ULA-based array design [20], we consider nonuniform linear array in this paper to avoid the lag redundancies intrinsically due to the uniform linear nature. We provide design examples that respectively achieve difference coarrays with a high number of consecutive correlation lags and a high number of unique correlation lags. For the latter, the rendered difference coarray does not have lag redundancies. Effective DOA estimation using group sparse reconstruction is demonstrated.

Notations: We use lower-case (upper-case) bold characters to denote vectors (matrices). In particular, \mathbf{I}_L denotes the $L \times L$ identity matrix. Notations $(\cdot)^T$ and $(\cdot)^H$ respectively denote the transpose and conjugate transpose of a matrix or vector, whereas $(\cdot)^*$ represents the complex conjugate operator. $\text{vec}(\cdot)$ stands for the vectorization operator that turns a matrix into a vector by stacking all columns on top of one another. $\|\cdot\|_2$ denotes the l_2 -norm of a vector, and $|\cdot|$ denotes the absolute value. $\mathbb{E}(\cdot)$ denotes the statistical expectation operator, and \otimes denotes the Kronecker product.

2. MULTI-FREQUENCY SENSOR ARRAY

2.1. Signal Model

In a multi-frequency sensor array, multiple continuous-wave (CW) signals with their respective frequencies of f_i , $i = 1, \dots, I$, are transmitted from a single transmit sensor or a phased array, which may be located at a distance. For the i th CW waveform with frequency f_i , the return signal vector scattered from the K far-field targets, respectively located at DOAs θ_k , $k = 1, 2, \dots, K$, is expressed as:

$$\tilde{\mathbf{x}}_i(t) = e^{j2\pi f_i t} \sum_{k=1}^K \rho_i^{(k)}(t) \mathbf{a}_i(\theta_k) + \tilde{\mathbf{n}}_i(t), \quad (1)$$

where $\rho_i^{(k)}(t)$ is the reflection coefficient which is in general frequency-dependent because both phase delay and target reflectivity vary with frequency. In addition, $\mathbf{a}_i(\theta_k)$ is the steering vector corresponding to θ_k expressed as:

$$\mathbf{a}_i(\theta_k) = \left[1, e^{-j\frac{2\pi d_1}{\lambda_i} \sin(\theta_k)}, \dots, e^{-j\frac{2\pi d_{L-1}}{\lambda_i} \sin(\theta_k)} \right]^T, \quad (2)$$

where $\lambda_i = c/f_i$ denotes the wavelength corresponding to frequency f_i , c is the velocity of wave propagation, d_l is the location of the l th element with respect to the reference sensor,

and L is the number of sensors. The sensor located at $l = 0$ is defined as the reference sensor, i.e., $d_0 = 0$. Furthermore, $\tilde{\mathbf{n}}_i(t) \sim \mathcal{CN}(0, \sigma_n^{(i)} \mathbf{I}_L)$ is the additive Gaussian noise vector, whose elements are assumed to be spatially and temporally white.

After downconverting the received signal vector to the baseband form through low-pass filtering, we obtain:

$$\mathbf{x}_i(t) = \sum_{k=1}^K \rho_i^{(k)}(t) \mathbf{a}_i(\theta_k) + \mathbf{n}_i(t) = \mathbf{A}_i \mathbf{p}_i(t) + \mathbf{n}_i(t), \quad (3)$$

where $\mathbf{A}_i = [\mathbf{a}_i(\theta_1), \dots, \mathbf{a}_i(\theta_K)]$ and $\mathbf{p}_i(t) = [\rho_i^{(1)}(t), \dots, \rho_i^{(K)}(t)]^T$.

2.2. Difference Coarray of Sparse Linear Array

We begin with the consideration of an L_0 -sensor ULA with interelement spacing d . The frequencies f_i , $i = 1, 2, \dots, I$, are chosen such that all M_i values are integer and satisfy $M_i \lambda_i / 2 = d$. Then, the set \mathbb{S}_i containing the sensor positions for the i th frequency are expressed as:

$$\mathbb{S}_i = \{M_i l \bar{d} \mid l \in \mathbb{P}\}, \quad (4)$$

where $\mathbb{P} = \{0, 1, 2, \dots, L_0 - 1\}$ and \bar{d} denotes half-wavelength in a normalized frequency sense (i.e., no specific frequency is referred to).

For multi-frequency array configurations based on a ULA, redundancies in the resulting difference coarray cannot be avoided [22]. Therefore, to achieve redundancy-free coarrays, in this paper, we consider sparse array designs by choosing l from $\mathbb{P}' \subset \mathbb{P}$ such that the cardinality of \mathbb{P}' is $L < L_0$. In this case, the sensor locations are given by:

$$\mathbb{S}_i = \{M_i l \bar{d} \mid l \in \mathbb{P}'\}. \quad (5)$$

The set \mathbb{S} of the combined sensor positions, incorporating the virtual sensors due to all I frequencies, is given as:

$$\mathbb{S} = \bigcup_{i=1}^I \mathbb{S}_i = \bigcup_{i=1}^I \{M_i l \bar{d} \mid l \in \mathbb{P}'\}. \quad (6)$$

Note that the reference sensors of all I arrays overlap at the zeroth position. Therefore, the number of unique virtual sensor positions is given by $|\mathbb{S}| \leq (L-1)I+1$, where the equality is achieved when all virtual sensors do not overlap except at the reference position.

Define the self-lag set as the different coarray sensor positions obtained from the same frequency, i.e.,

$$\mathbb{C}_{\text{self}} = \bigcup_{u=1}^I \mathbb{S}_u \ominus \mathbb{S}_u = \bigcup_{u=1}^I \{M_u(l_1 - l_2) \bar{d}\}, \quad (7)$$

where \ominus computes the lags between two sets. Similarly, the corresponding cross-lags are obtained from the different frequency pairs, defined as

$$\mathbb{C}_{\text{cross}} = \bigcup_{\forall u, v, u \neq v} \mathbb{S}_u \ominus \mathbb{S}_v = \bigcup_{\forall u, v, u \neq v} \{(M_u l_1 - M_v l_2) \bar{d}\}, \quad (8)$$

where $l_1, l_2 \in \mathbb{P}'$ and $1 \leq u, v \leq I$. The complete set of the coarray positions constituting all the correlation lags are represented by $\mathbb{C} = \mathbb{C}_{\text{self}} \cup \mathbb{C}_{\text{cross}}$, and the corresponding set of all non-negative correlation lags is denoted as \mathbb{C}^+ .

2.3. Remarks

The multi-frequency sensor array considered in this paper shares similar spirit with the coprime and nested arrays such that multiple subarrays are formed, rendering effective construction of difference coarrays. However, they differ in several ways: (a) Comparing to coprime and nested arrays which require multiple physical subarrays, a multi-frequency array uses a single physical array and thus is much more economically beneficial; (b) Unlike coprime and nested arrays where the two subarrays may have different numbers of array sensors, the subarrays in a multi-frequency array stem from the same physical array and thus have the same number of L sensors; (c) Since the target reflection coefficient $\rho_i^{(k)}(t)$ is frequency-dependent, we cannot directly compute the correlation and determine the phase difference between the data observed at different frequencies. Processing of the data observed at different frequencies can be effectively carried out using group sparse reconstruction methods [20, 22, 25, 27] and is summarized in Section 4; (d) The array designs considered in this paper differ to the multi-frequency coprime arrays considered in [20, 22] because the physical arrays are not uniform linear to render redundancy-free coarrays.

3. DESIGN EXAMPLES

In this section, we provide three design examples, all using $L = 3$ sensors and $I = 3$ frequencies. In all examples, the relative bandwidth given by $2(f_3 - f_1)/(f_3 + f_1)$ is set to 40%. In this case, the highest frequency is given by $f_3 = 3f_1/2$, whereas different values of f_2 will be considered. Extension to scenarios with more sensors, more frequencies, or a different bandwidth is straightforward.

3.1. Design Example 1: High number of consecutive lags

In the first example, we select $f_2 = 5f_1/4$ so that the three carrier frequencies are equally spaced. To avoid fractional half-wavelength spacing, we select the sensor positions as:

$$\mathbb{S}_1 = \{0, 4, 12\} \lambda_1 / 2, \quad (9)$$

i.e., $M_1 = 4$ and $\mathbb{P}' = \{0, 1, 3\}$. From the frequency ratios, we have $M_2 = f_2 M_1 / f_1 = 5$ and $M_3 = f_3 M_1 / f_1 = 6$. The resulting virtual sensor positions corresponding to these two frequencies are expressed as:

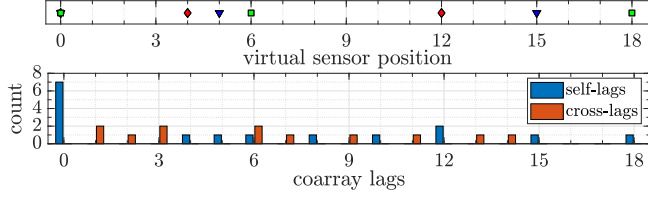
$$\mathbb{S}_2 = \{0, 5, 15\} \lambda_2 / 2, \quad \mathbb{S}_3 = \{0, 6, 18\} \lambda_3 / 2. \quad (10)$$

Collecting all virtual sensor positions and expressing them in terms of half-wavelength \bar{d} , regardless of the actual frequency, we obtain the collective sensor positions as:

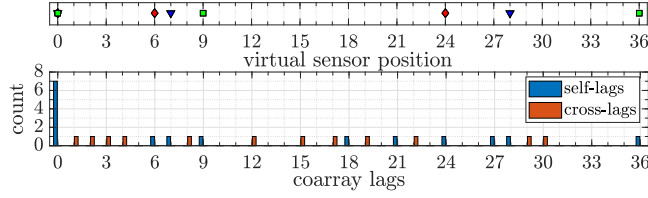
$$\mathbb{S} = \mathbb{S}_1 \cup \mathbb{S}_2 \cup \mathbb{S}_3 = \{0, 4, 5, 6, 12, 15, 18\} \bar{d}. \quad (11)$$

The yielding non-negative difference coarray positions of the correlation lags are given as:

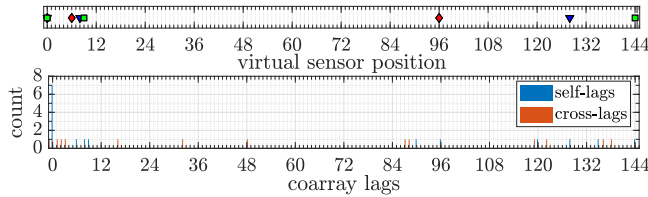
$$\mathbb{C}^+ = \{0, 1, 2, 3, 4, 5, 6, 7, 8, 9, 10, 11, 12, 13, 14, 15, 18\} \bar{d}. \quad (12)$$



(a) Design Example 1: High number of consecutive lags



(b) Design Example 2: High number of unique lags



(c) Design Example 3: Excessively large array aperture

Fig. 1. Virtual sensor positions and the histogram of corresponding non-negative difference coarray lags.

For this case, the collective sensor positions and the coarray positions are illustrated in Fig. 1(a) using Eqs. (7) and (8). Note that the lags with respect to the reference sensor for different frequencies are counted only once. We observe in Fig. 1(a) that the number of non-negative consecutive lags is 16, and the number of non-negative unique lags is 17. Considering the fact that we only use three physical sensors, the coarray obtained from this design is impressive. On the other hand, due to the equal separation between the three carrier frequencies, there are redundancies in multiple difference coarray sensor positions (at lags 1, 3, 6, and 12). For instance, consider the lag 6, one self-lag exists due to the $\{0\bar{d}, 6\bar{d}\}$ pair in \mathbb{S}_3 , and two cross-lags are rendered due to the difference between the $\{6\bar{d}, 12\bar{d}\}$ pair and the $\{12\bar{d}, 18\bar{d}\}$ pair between \mathbb{S}_1 and \mathbb{S}_3 . Such redundancies can be avoided by using sparse nonlinear arrays as illustrated in Design Examples 2 and 3.

3.2. Design Example 2: High number of unique lags

In this example, we choose $f_2 = 7f_1/6$ so that the three frequencies are unequally spaced. We also modify the inter-element spacing such that there are no lag redundancies. The sensors positions chosen for the first frequency are:

$$\mathbb{S}_1 = \{0, 6, 24\}\lambda_1/2, \quad (13)$$

and the corresponding sensor locations at the other two frequencies become:

$$\mathbb{S}_2 = \{0, 7, 28\}\lambda_2/2, \quad \mathbb{S}_3 = \{0, 9, 36\}\lambda_3/2. \quad (14)$$

As a result, the collective sensor positions are given by:

$$\mathbb{S} = \mathbb{S}_1 \cup \mathbb{S}_2 \cup \mathbb{S}_3 = \{0, 6, 7, 9, 24, 28, 36\}\bar{d}. \quad (15)$$

The corresponding non-negative difference coarray positions are obtained as:

$$\mathbb{C}^+ = \{0, 1, 2, 3, 4, 6, 7, 8, 9, 12, 15, 17, 18, 19, 21, 22, 24, 27, 28, 29, 30, 36\}\bar{d}. \quad (16)$$

The collective sensor positions and the difference coarray positions are shown in Fig. 1(b). This design does not provide a high number of consecutive lags, but achieves the highest number of unique lags (i.e., 22 non-negative lags), as there are no redundancies in all lags except the unavoidable ones for lag 0. Moreover, the array aperture is higher than that of Design Example 1.

3.3. Design Example 3: Excessively large array

The third example presents an array design that also exhibits no lag redundancies but has a much larger array aperture. We choose unequally spaced frequencies with $f_2 = 4f_1/3$. The sensor positions considered for the first frequency in this example are given by:

$$\mathbb{S}_1 = \{0, 6, 96\}\lambda_1/2, \quad (17)$$

and the corresponding sensor locations at the other two frequencies are given as:

$$\mathbb{S}_2 = \{0, 8, 128\}\lambda_2/2, \quad \mathbb{S}_3 = \{0, 9, 144\}\lambda_3/2. \quad (18)$$

The collective sensor positions become:

$$\mathbb{S} = \mathbb{S}_1 \cup \mathbb{S}_2 \cup \mathbb{S}_3 = \{0, 6, 8, 9, 96, 128, 144\}\bar{d}, \quad (19)$$

and the non-negative difference coarray positions for this array design are obtained as:

$$\mathbb{C}^+ = \{0, 1, 2, 3, 6, 8, 9, 16, 32, 48, 87, 88, 90, 96, 119, 120, 122, 128, 135, 136, 138, 144\}\bar{d}. \quad (20)$$

The collective sensor positions and the resulting difference coarray positions are shown in Fig. 1(c). This array design achieves 22 unique lags which is the same as Design Example 2. However, this array is sparser and has a much larger aperture. Compared to Design Example 2, it is expected that this array provides a higher resolution but may yield higher sidelobe effects.

4. GROUP SPARSITY-BASED DOA ESTIMATION

In this section, we address the DOA estimation by employing the group lasso algorithm [27]. In this context, we construct the correlation matrices of the received signals at the array by exploiting Eq. (3) as follows:

$$\hat{\mathbf{R}}_{u,v} = \frac{1}{T} \sum_{t=1}^T \mathbf{x}_u(t) \mathbf{x}_v^H(t) \approx \mathbf{A}_u \mathbf{P} \mathbf{A}_v + \sigma_n^2 \mathbf{I}_L. \quad (21)$$

The different combinations of u and v values in the above equation result in L^2 correlation matrices from the received

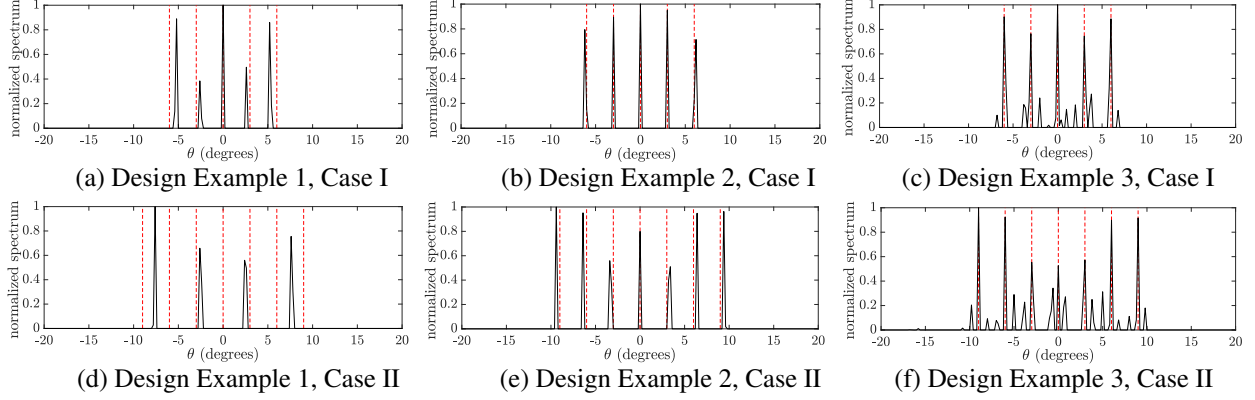


Fig. 2. Group sparsity-based DOA estimation performance for the array structures under consideration.

array data corresponding to the I frequencies. By vectorizing the correlation matrices, we obtain [22, 25]:

$$\mathbf{z}_{u,v} = \text{vec}(\hat{\mathbf{R}}_{u,v}) = \tilde{\mathbf{A}}_{u,v} \mathbf{r}_{u,v} + \sigma_n^2 \tilde{\mathbf{1}}, \quad (22)$$

where $\tilde{\mathbf{A}}_{u,v} = [\tilde{\mathbf{a}}_{u,v}(\theta_1), \dots, \tilde{\mathbf{a}}_{u,v}(\theta_K)]$ with $\tilde{\mathbf{a}}_{u,v}(\theta_k) = \mathbf{a}_u^*(\theta_k) \otimes \mathbf{a}_v(\theta_k)$, and $\tilde{\mathbf{1}} = \text{vec}(\mathbf{I}_L)$. In addition, $\mathbf{r}_{u,v} = \mathbb{E}\{[\rho_u^{(1)}(t)(\rho_v^{(1)}(t))^*, \dots, \rho_u^{(K)}(t)(\rho_v^{(K)}(t))^*]^T\}$. We consider uncorrelated targets such that $\mathbb{E}\{\rho_u^{(k_1)}(t)\rho_v^{(k_2)}(t)\} = 0, \forall k_1 \neq k_2$.

For group sparsity-based lasso, we introduce I^2 optimization vectors $\mathbf{r}_{u,v}^o$ of size $G \times 1$, where G is the search grid for DOAs. The dictionary matrix for the G -point search grid corresponding to $\tilde{\mathbf{A}}_{u,v}$ is given by $\mathbf{B}_{u,v}$. The resulting group sparse optimization is formulated as [27, 28]:

$$\hat{\mathbf{r}}_{u,v}^o = \arg \min_{\mathbf{r}_{u,v}^o} \sum_{u=1}^I \sum_{v=1}^I \|\mathbf{z}_{u,v} - \mathbf{B}_{u,v} \mathbf{r}_{u,v}^o\|_2 + \zeta \|\mathbf{r}_{u,v}^o\|_{1,2}, \quad (23)$$

where ζ is the regularization parameter and the mixed $\ell_{1,2}$ -norm is given by:

$$\|\mathbf{r}_{u,v}^o\|_{1,2} = \sum_{a=1}^G \left(\sum_{b=1}^{I^2} \mathcal{R}(a,b) \mathcal{R}^*(a,b) \right)^{0.5}. \quad (24)$$

Here, \mathcal{R} is a matrix constructed by concatenating all the vectors $\mathbf{r}_{u,v}^o$ whereas $\mathcal{R}(a,b)$ denotes its element located at the a th row and the b th column. The final G -point grid of DOA estimates is obtained as:

$$\hat{\mathbf{r}} = \sum_{u=1}^I \sum_{v=1}^I |\hat{\mathbf{r}}_{u,v}^o|. \quad (25)$$

5. SIMULATION RESULTS

In this section, we present simulation results illustrating the DOA estimation performance for the three design examples discussed in Section 4. In all the simulations, the input signal-to-noise ratio is kept at 0 dB and 10,000 data snapshots are taken. All targets are assumed to be uncorrelated.

Case I: In this case, we assume 5 signals that are uniformly spaced between -6° and 6° . Fig. 2(a) illustrates the DOA estimation results for Design Example 1. Note that the

array structure resolves all the sources successfully. However, a bias in the estimates is observed, implying the low resolution performance of this array design. Fig. 2(b) shows the superior DOA estimation results for this case using Design Example 2 which achieves the highest number of unique lags. The result of Design Example 3 in Fig. 2(c) shows similar performance but with clear spurious peaks in the estimates due to the high sidelobe effects of this highly sparse array design.

Case II: In this case, we consider 7 sources that are uniformly spaced between -9° and 9° . For this case, the DOA estimates for Design Example 1, shown in Fig. 2(d), fail to resolve all the sources due to its small number of unique lags and smaller array aperture. Fig. 2(e) shows the DOA estimation results for Design Example 2 which successfully resolves all the sources due to its high number of unique lags and much larger array aperture, leading to significantly improved resolution capabilities. The results for design Example 3, shown in Fig. 2(f), present more accurate DOA estimates but the estimated spectrum is highly distorted by the large number of spurious peaks.

These examples illustrate that the number of unique lags and the array aperture play an important role in DOA estimation performance for multi-frequency arrays. Adequate design of the array geometry and appropriate frequency selection allow us to trade off between the spatial resolution and spurious peaks. On the other hand, the number of consecutive lags is less important in this design because subspace-based DOA estimation methods, e.g., MUSIC, do not directly apply.

6. CONCLUSION

We presented the multi-frequency sparse array concept that achieves effective sparse array with desirable difference coarrays. It is demonstrated through analysis and design examples that a careful combination of nonuniform linear array and unequally spaced frequencies enables redundancy-free difference coarrays and thus achieves a high number of unique correlation lags. The selection of different array apertures trades off between the achieved spatial resolution and the likelihood of having spurious peaks in the resulting spectrum.

7. REFERENCES

- [1] A. Moffet, "Minimum-redundancy linear arrays," *IEEE Trans. Antennas Propag.*, vol. 16, no. 2, pp. 172–175, March 1968.
- [2] R. T. Hoctor and S. A. Kassam, "The unifying role of the co-array in aperture synthesis for coherent and incoherent imaging," *Proc. IEEE*, vol. 78, no. 4, pp. 735–752, April 1990.
- [3] P. Pal and P. P. Vaidyanathan, "Nested arrays: A novel approach to array processing with enhanced degrees of freedom," *IEEE Trans. Signal Process.*, vol. 58, no. 8, pp. 4167–4181, Aug. 2010.
- [4] P. P. Vaidyanathan and P. Pal, "Sparse sensing with co-prime samplers and arrays," *IEEE Trans. Signal Process.*, vol. 59, no. 2, pp. 573–586, Feb. 2011.
- [5] P. Pal and P. P. Vaidyanathan, "Coprime sampling and the MUSIC algorithm," in *Proc. IEEE Digit. Signal Process. Workshop/IEEE Signal Process. Educ. Workshop*, Sedona, AZ, Jan. 2011, pp. 289–294.
- [6] S. Qin, Y. D. Zhang, and M. G. Amin, "Generalized coprime array configurations for direction-of-arrival estimation," *IEEE Trans. Signal Process.*, vol. 63, no. 6, pp. 1377–1390, March 2015.
- [7] C.-L. Liu and P. P. Vaidyanathan, "Super nested arrays: Linear sparse arrays with reduced mutual coupling – Part I: Fundamentals," *IEEE Trans. Signal Process.*, vol. 64, no. 15, pp. 3997–4012, Aug. 2016.
- [8] C.-L. Liu and P. P. Vaidyanathan, "Super nested arrays: Linear sparse arrays with reduced mutual coupling – Part II: High-Order Extensions," *IEEE Trans. Signal Process.*, vol. 64, no. 16, pp. 4203–4217, Aug. 2016.
- [9] A. Ahmed, Y. D. Zhang, and B. Himed, "Effective nested array design for fourth-order cumulant-based DOA estimation," in *Proc. IEEE Radar Conf.*, Seattle, WA, May 2017, pp. 998–1002.
- [10] W. Wang, S. Ren, and Z. Chen, "Unified coprime array with multi-period subarrays for direction-of-arrival estimation," *Digital Signal Process.*, vol. 74, pp. 30–42, March 2018.
- [11] Y.-K. Zhang, H.-Y. Xu, R. Zong, B. Ba, and D.-M. Wang, "A novel high degree of freedom sparse array with displaced multistage cascade subarrays," *Digital Signal Process.*, vol. 90, pp. 36–45, July 2019.
- [12] C. Li, L. Gan, and C. Ling, "Coprime sensing via Chinese remaindering over quadratic fields — Part I: Array design," *IEEE Trans. Signal Process.*, vol. 67, no. 11, pp. 2898–2910, June 2019.
- [13] Z. Zheng, W.-Q. Wang, Y. Kong, and Y. D. Zhang, "MISC Array: A new sparse array design achieving increased degrees of freedom and reduced mutual coupling effect," *IEEE Trans. Signal Process.*, vol. 67, no. 7, pp. 1728–1741, April 2019.
- [14] S. Qin, Y. D. Zhang, and M. G. Amin, "Improved two-dimensional DOA estimation using parallel coprime arrays," *Signal Process.*, in press.
- [15] A. Ahmed, Y. D. Zhang, and J.-K. Zhang, "Coprime array design with minimum lag redundancy," in *Proc. IEEE Int. Conf. Acoust. Speech Signal Process.*, Brighton, U.K., May 2019, pp. 4125–4129.
- [16] Y. Liu and J. R. Buck, "High-resolution Direction-of-Arrival estimation in SNR and snapshot challenged scenarios using multi-frequency coprime arrays," in *Proc. IEEE Int. Conf. Acoust. Speech Signal Process.*, New Orleans, LA, March 2017, pp. 3434–3438.
- [17] Y. D. Zhang, M. G. Amin, and B. Himed, "Sparsity-based DOA estimation using co-prime arrays," in *Proc. IEEE Int. Conf. Acoust. Speech Signal Process.*, Vancouver, Canada, May 2013, pp. 3967–3971.
- [18] Q. Shen, W. Liu, W. Cui, S. Wu, Y. D. Zhang, M. G. Amin, "Low-complexity direction-of-arrival estimation based on wideband co-Prime arrays," *IEEE/ACM Trans. Audio, Speech Lang. Process.*, vol. 23, no. 9, pp. 1445–1456, Sept. 2015.
- [19] C. Zhou, Y. Gu, Z. Shi, and Y. D. Zhang, "Off-grid direction-of-arrival estimation using coprime array interpolation," *IEEE Signal Process. Lett.*, vol. 25, no. 11, pp. 1710–1714, Nov. 2018.
- [20] Y. D. Zhang, M. G. Amin, F. Ahmad, and B. Himed, "DOA estimation using a sparse uniform linear array with two CW signals of co-prime frequencies," in *Proc. IEEE Int. Workshop Comput. Adv. in Multi-Sensor Adaptive Process.*, Saint Martin, Dec. 2013, pp. 404–407.
- [21] S. Qin, Y. D. Zhang, and M. G. Amin, "DOA estimation exploiting coprime frequencies," in *Proc. SPIE*, vol. 9103, no. 91030E, Baltimore, MD, May 2014.
- [22] S. Qin, Y. D. Zhang, M. G. Amin, and B. Himed, "DOA estimation exploiting a uniform linear array with multiple coprime frequencies," *Signal Process.*, vol. 130, pp. 37–46, Jan. 2017.
- [23] M. Guo, Y. D. Zhang, and T. Chen, "Compressive measurements exploiting coprime frequencies for direction finding," in *Proc. IEEE Sensor Array and Multichannel Signal Process. Workshop*, Sheffield, U.K., July 2018, pp. 26–30.
- [24] A. Liu, X. Zhang, Q. Yang, and W. Deng, "Fast DOA estimation algorithms for sparse uniform linear array with multiple integer frequencies," *IEEE Access*, vol. 6, pp. 29952–29965, May 2018.
- [25] A. Ahmed, Y. D. Zhang, and B. Himed, "Cumulant-based direction-of-arrival estimation using multiple co-prime frequencies," in *Proc. Asilomar Conf. Signals, Syst., Comput.*, Pacific Grove, CA, Oct. 2017, pp. 1188–1192.
- [26] M. Guo, Y. D. Zhang, and T. Chen, "Performance analysis for uniform linear arrays exploiting two coprime frequencies," *IEEE Signal Process. Lett.*, vol. 25, no. 6, pp. 838–842, June 2018.
- [27] L. Meier, S. V. D. Geer, and P. Bühlmann, "The group lasso for logistic regression," *J. R. Statist. Soc. B*, vol. 70, no. 1, Feb. 2008, pp. 53–71.
- [28] N. Simon and R. Tibshirani, "Standardization and the group lasso penalty," *Stat. Sin.*, vol. 22, no. 3, pp. 983–1001, June 2012.